

RETHINKING MEMORY AND COMMUNICATION COST FOR EFFICIENT LARGE LANGUAGE MODEL TRAINING

Chan Wu¹ Hanxiao Zhang¹ Lin Ju¹ Jinjing Huang¹ Youshao Xiao¹ Zhaoxin Huan¹ Siyuan Li¹
 Fanzhuang Meng¹ Lei Liang¹ Xiaolu Zhang¹ Jun Zhou¹

ABSTRACT

As model sizes and training datasets continue to increase, large-scale model training frameworks reduce memory consumption by various sharding techniques. However, the huge communication overhead reduces the training efficiency, especially in public cloud environments with varying network bandwidths. In this paper, we rethink the impact of memory consumption and communication overhead on the training speed of large language model, and propose a memory-communication balanced Partial Redundancy Optimizer (PaRO). PaRO reduces the amount and frequency of inter-group communication by grouping GPU clusters and introducing minor intra-group memory redundancy, thereby improving the training efficiency of the model. Additionally, we propose a Hierarchical Overlapping Ring (HO-Ring) communication topology to enhance communication efficiency between nodes or across switches in large model training. Our experiments demonstrate that the HO-Ring algorithm improves communication efficiency by 32.6% compared to the traditional Ring algorithm. Compared to the baseline ZeRO, PaRO significantly improves training throughput by 1.2x-2.6x and achieves a near-linear scalability. Therefore, the PaRO strategy provides more fine-grained options for the trade-off between memory consumption and communication overhead in different training scenarios.

1 INTRODUCTION

With the development of machine learning technology, the overall performance of deep learning algorithms in fields such as autonomous driving, face recognition, and natural language processing has significantly improved. Recent research shows that large model training is beneficial to improve model quality. Over the past few years, model size has increased from 110 million parameters for BERT (Devlin et al., 2019) to 175 billion parameters for GPT-3 (Brown et al., 2020). However, training such large-scale artificial intelligence models is not an easy task, as it requires a significant amount of computing resources and presents challenges in terms of system complexity.

As the size of the model and the amount of training data continue to increase, the computing power of a single GPU cannot meet the training needs of large-scale networks. In large-scale model training, in order to effectively utilize the computing power and memory of hundreds of GPU devices, a variety of distributed parallel training technologies have been proposed, such as data parallelism (DP), tensor parallelism (TP) and pipeline parallelism (PP) (Li et al., 2023). In DP, an entire dataset is evenly partitioned into mutually exclusive subsets before training, and each worker works on a separate subset of them. TP divides the calculation and memory load of a single layer onto multiple GPUs by modifying the calculation method within the layer. PP puts different layers on different GPUs, and then divides the computing and memory loads onto multiple GPUs. However, TP, PP and SP require modification of the model structure, which is difficult to implement. In contrast, data parallelism has become the most mainstream distributed parallel method due to its simplicity and ease of operation.

In data parallelism, the replicated model on each GPU processes a portion of the input batch, resulting in a large amount of communication data when fusing gradients. A ring all-reduce method (Proffici, 2018) is proposed to balance communication load. By defining the communication topology, the communication pressure is evenly distributed to each GPU. This communication volume is a fixed constant and is not affected by the number of GPUs, thus achieving cross-machine data parallelism. However, since a complete model is copied on each GPU, significant memory redundancy occurs, especially when training large models. To this end, Rajbhandari et al. (Rajbhandari et al., 2020) proposed the Zero Redundancy Optimization (ZeRO) framework, which splits the model state (i.e. optimizer state,

¹Ant Group, Beijing, Chaoyang, China. Correspondence to: Chan Wu <wuchan.wu@antgroup.com>, Lin Ju <julin.jl@antgroup.com>.

gradient and parameters) based on data parallelism and reconstructs them through the collective communication. This approach reduces memory overhead during training of large models, thereby improving training efficiency and scalability.

Since ZeRO retains the simplicity, ease of use, and versatility of DP, it has been widely used in large-scale model training. ZeRO needs to be adapted to specific training frameworks and hardware equipment to fully exploit its advantages. In high-performance clusters such as NVIDIA DGX-2 or DGX-A100 (Wang et al., 2020), nodes are configured with NVLink/NVSwitch with high bandwidth up to 4.8Tbps, while the bandwidth of InfiniBand or Ethernet between nodes is only 200~800Gbps. The mismatch of bandwidth within and between nodes limits the training efficiency of ZeRO. In order to speed up model training, ZeRO requires more GPU resources, which will result in greater collective communication volume. Multiple fragmented communications reduce overall bandwidth utilization. To reduce collective communication volume, the MiCS (Zhang et al., 2022) system proposes a clustering grouping strategy, where all model states are partitioned within each group and replicated across different groups. However, this coarse-grained partitioning strategy incurs significant memory overhead, particularly in scenarios with a large number of groups.

In this paper, we group cluster GPUs and define three sharding granularities according to the sharding range of the model state: no sharding, intra-group sharding and global sharding. Based on the memory usage and synchronization frequency of the optimizer state, gradients and parameters in the model state, we designed three sharding criteria and three optimization solutions for ZeRO. These solutions aim to reduce overall communication volume and frequency with minimal memory overhead, thereby improving the training efficiency of the model. Additionally, we optimize the communication topology of ring all-gather and reduce-scatter operations by performing intra-node and inter-node communication in steps. This strategy reduces inter-node communication volume and improves inter-node bandwidth utilization.

The main contributions of the paper are as follows:

- We analyzed the impact of memory usage and communication overhead on the training speed of large models, and proposed an overall guideline for balancing memory and communication.
- We proposed a Hierarchical Overlapping Ring (HO-Ring) communication topology for inter-node or cross-switch communication scenarios in large model training. Compared with the traditional Ring, the communication efficiency of the HO-Ring is increased by 32.6%.

- We proposed the Partial Redundancy Optimizer (PaRO) strategy set, which provides more refined options for the trade-off between memory usage and communication overhead in different training scenarios.
- Compared with the baseline ZeRO, PaRO significantly improves training throughput by 1.2x-2.6x and has a higher acceleration ratio, especially in network environments with large intra- and inter-group bandwidth differences.

2 BACKGROUND AND RELATED WORKS

2.1 Data, Tensor and Pipeline Parallelism

According to different parallel objects, distributed parallel training technology can be divided into data parallelism and model parallelism (Korthikanti et al., 2023). Model parallelism, in particular, slices the model structure or model parameters to ensure that each GPU only retains a portion of the model state. It can be further divided into tensor parallelism (split within model layers) and pipeline parallelism (split between model layers).

Data parallelism divides the input data equally into several shards and assigns them to different GPUs. Each GPU owns the complete replica of model parameters. After forward and backward computations, each GPU obtains the corresponding parameter gradients. These gradients are then aggregated and transmitted back to each GPU through the all-reduce operation. Finally, the model parameters are updated based on the gradient and optimizer state (Sergeev & Balso, 2018). Data parallelism simplifies model training and deployment, but it requires each GPU to maintain a complete replica of the model state. However, the approach may not meet the memory requirements of large-scale models, especially when using the Adam optimizer (Kingma & Ba, 2017). Additionally, the communication overhead during gradient transmission increases almost linearly with the number of GPUs, making the network bandwidth a bottleneck for training efficiency .

Tensor parallelism shards tensors onto multiple GPU devices by modifying the model structure, and implements model parallelism through distributed matrix multiplication. Based on the characteristics of the Transformer architecture, Megatron-LM (Shoeybi et al., 2020) divides the layers in the row or column dimension to achieve 1D tensor parallelism. Since the output of each layer in 1D tensor parallelism is incomplete, an all-gather operation is required to aggregate the complete input before passing it to the next layer. In this process, the collective communication of 1D tensor parallelism generates a large amount of communication overhead. Low bandwidth between nodes will affect the efficiency of 1D tensor parallel training. Additionally, 1D tensor parallelism incurs redundant memory overhead due to repeated inputs to

each layer and repeated outputs after all-reduce. To address these issues, more advanced tensor parallelism methods, such as 2D (Xu & You, 2023), 2.5D (Wang et al., 2021), and 3D (Bian et al., 2021) tensor parallelism, have been introduced in LLM training. These methods shard the initial inputs using distributed matrix multiplication (Solomonik & Demmel, 2011; Agarwal et al., 1995), which eliminates communication in the middle layer and only requires one all-gather communication in the last layer. These improved tensor parallelism algorithms can be combined with pipeline parallelism methods.

Pipeline parallelism distributes different layers of the model across different GPUs and implements pipeline processing by splitting the input batch into mini-batches (Narayanan et al., 2021; Fan et al., 2021). Theoretically, the reduced memory in pipeline parallelism is directly proportional to the number of pipeline stages. This feature allows the model size to scale linearly with the number of GPUs. However, pipeline parallelism does not reduce the memory footprint of the activation functions in each layer. As the model size increases, the intermediate results stored in each GPU will also become larger. To mitigate memory overhead, Gpipe (Huang et al., 2019) utilizes the re-materialization mechanism, which avoids caching intermediate results in forward propagation and recomputes them in backward propagation. In practical applications, the balance of model sharding among nodes affects the overall computational efficiency.

2.2 ZeRO Optimizer

The training process of deep learning models mainly consists of three stages: forward computation, backward computation, and parameter update. During the training process, GPUs need to store both model states and activations. ZeRO (Rajbhandari et al., 2020) primarily reduces the memory consumption of model states, which mainly include model parameters, gradients from backward computation, and optimizer states for parameter updates. Based on data parallelism, ZeRO gradually optimizes redundant memory in three stages: ZeRO-1 only shards optimizer states; ZeRO-2 shards gradients and optimizer states; ZeRO-3 shards model parameters, gradients, and optimizer states.

ZeRO-1 utilizes a greedy strategy to shard the optimizer state, and each GPU saves an approximately equal-sized shard. During the training process, each GPU performs forward computation and backward computation independently to obtain the gradient, which are then synchronized among all GPUs using the all-reduce operation. Since each GPU retains a shard of the optimizer state, only the corresponding model parameters can be updated. After that, the updated model parameter shards are retrieved from other GPUs using the all-gather operation to ensure that all GPUs

have the latest model parameters.

Compared to ZeRO-1, ZeRO-2 not only shards the optimizer state but also shards the gradient. During the training process, each GPU stores a complete set of model parameters and independently performs forward computation and backward computation to obtain a gradient. Afterwards, each GPU updates the gradient shards through the reduce-scatter operation and discards the other gradient shards. The subsequent processes remain the same as in ZeRO-1.

In ZeRO-3, model parameters, gradients, and optimizer state are all sharded. Before performing forward and backward computations, each GPU performs an all-gather operation to collect model parameter shards from other GPUs and construct the complete model parameters. After gradient calculation, each GPU immediately discards the model parameter slices that it does not maintain. Afterwards, each GPU updates its corresponding model parameter shards using the optimizer parameter shards and gradient shards it maintains. Since each GPU only maintains one model parameter shard, there is no need for an all-reduce operation.

To further reduce GPU memory usage, ZeRO-Offload (Ren et al., 2021) and ZeRO-Infinity (Rajbhandari et al., 2021) offload optimizer states to CPU memory or NVMe SSD, which can be used for training larger models. Similarly, the PyTorch’s official Fully Sharded Data Parallel (FSDP) (Zhao et al., 2023) framework flattens and shards all model parameters across all data parallel workers, and supports CPU offloading.

2.3 Communication Overhead

For models with billions to trillions of parameters, ZeRO-3 transfers a significant amount of data ranging from tens to hundreds of gigabytes during forward computation, backward computation, and gradient updates. Unlike DGX systems and local clusters, the network bandwidth between GPU nodes in public cloud is limited, and the network topology cannot be controlled by the users. As a result, the inter-node network performance tends to be worse in public cloud. Furthermore, as the cluster size grows, each GPU needs to communicate multiple times, which amplifies the latency of collective communication operation. Therefore, an efficient communication topology is crucial to reduce the communication overhead of the overall operation.

Taking the all-reduce as an example, the traditional ring all-reduce fails to consider the differences in intra- and inter-node network bandwidth, thereby unable to fully utilize the bandwidth of clusters. Hierarchical ring all-reduce (Jia et al., 2018) groups GPUs based on their respective nodes and improves the efficiency of the ring all-reduce through the communication topology of intra-group reduce, inter-group all-reduce, and intra-group broadcast. However, in

inter-group all-reduce, only one GPU of each node participates in communication, resulting in low inter-group bandwidth utilization. To address this issue, Mikami et al. (Mikami et al., 2018) proposed the 2D-Torus all-reduce scheme, where the communication topology is modified into intra-group reduce-scatter, inter-group all-reduce and intra-group all-gather. While the total communication volume of 2D-Torus all-reduce is the same as hierarchical ring all-reduce, 2D-Torus is more efficient due to the simultaneous communication of all GPUs in inter-group all-reduce.

To reduce the cost of inter-node communication, MiCS (Zhang et al., 2022) divides the GPU cluster into subgroups, where the model state is partitioned within the subgroups and replicated across the subgroups. By configuring suitable subgroup sizes, MiCS can leverage the high intra-node bandwidth and a hierarchical communication strategy to reduce the communication volume between nodes. Similarly, the ZeRO++ (Wang et al., 2023) system performs a secondary sharding of parameters while keeping other model states sharded across all GPUs to reduce inter-node communication overhead. In addition, ZeRO++ compresses model parameters and gradients through quantization to reduce inter-node communication volume and latency. Additionally, FSDP (Zhao et al., 2023) provides two hybrid sharding strategies: HYBRID-SHARD (FSDP-hs) and HYBRID-SHARD-ZERO2 (FSDP-hsZ2), which leverage data center locality to accelerate training and reduce inter-node communication. This approach provides a progressive trade-off between memory reduction and throughput improvements.

3 SYSTEM OVERVIEW AND DESIGN

3.1 Notation

We define the notations used in this section as follows:

N : Number of GPUs in the cluster.

M : Number of GPUs in the group or node.

g : Number of groups or nodes, $g = N/M$.

s : Step of gradient accumulations.

K : Optimizer parameters.

Ψ : Number of model parameters.

Ψ' : Number of trainable parameters.

P : Parameter.

G : Gradient.

OS : Optimizer state.

3.2 Insights

Data-parallel training requires collective communication between GPUs. While computation-communication overlap techniques are widely used, collective communication

remains a bottleneck for overall training speed, especially in clusters with a large-scale GPU nodes. In the cluster, the communication bandwidth within a node is much larger than the communication bandwidth between nodes, but the communication delay within a node is much lower than the communication delay between nodes. Therefore, the communication bottleneck in training mainly lies in the communication between nodes. The bottleneck of collective communication in training is summarized as follows:

- When $\Psi \approx \Psi'$, the bottleneck lies in the inter-node communication bandwidth.
- When $\Psi \gg \Psi'$ (e.g., LoRA, P-tuning, etc.), the bottleneck lies in the the delay of communication operations between nodes.

During the training process, model states mainly include model parameters, gradients, and optimizer states. In the scenario of mixed precision (Kingma & Ba, 2017), the three components consume 2Ψ , $2\Psi'$, and $12\Psi'$ memory, respectively. ZeRO shards the model state at different levels, and each GPU only maintains a part of the shards to reduce memory redundancy. The memory consumption of various ZeRO can be ranked as $ZeRO1 > ZeRO2 > ZeRO3$. Due to the introduction of group sharding strategy, the memory consumption of MiCS is between ZeRO2 and ZeRO3. The principle of sharding model state from the perspective of saving memory is summarized as follows:

- When $\Psi \approx \Psi'$, we shard the optimizer states first, then the gradients, and finally the model parameters.
- When $\Psi \gg \Psi'$, we shard the model parameters first, then the optimizer states, and finally the gradients.

The number of collective communication participants can be reduced by grouping GPUs in the cluster and retaining a partial memory redundancy. To fully leverage the communication bandwidth advantage of a heterogeneous network, GPU clusters are generally grouped according to nodes. Therefore, intra- and inter-group bandwidth correspond to intra- and inter-node bandwidth respectively. We define three sharding granularities according to the sharding scope of the model state: no sharding, intra-group sharding and global sharding. In the case of gradient accumulation, the impact of different model state sharding on communication overhead is summarized as follows:

- **Gradient sharding:** Before the forward calculation of each micro-batch, an all-gather is required to obtain all parameters of the current layer. When sharding model parameters within a group, only intra-group all-gather is required.
- **Parameter sharding:** In the backward computation of each micro-batch, the aggregated gradient of the

corresponding local shard is obtained through collective communication. When sharding gradients within a group, only intra-group reduce-scatter is required. At the end of the mini-batch, another collective communication is performed based on the sharding scope of the optimizer state.

- **Optimizer state sharding:** If the sharding scope for optimizer states and parameters is different, collective communication operations are required to update parameters of the local shards. Since the total communication volume and inter-group communication volume of the sharded optimizer state are the same for both unsharded and global sharded optimizer states, it is meaningless to leave the optimizer state unsharded. When the optimizer state is sharded within the group, the update process first performs an intra-group reduce-scatter and then an all-reduce on Ψ'/M across k GPUs. When $2\Psi'/M < \Psi'$, $M > 2$ (GPU servers typically have 4 or more GPUs), its communication cost is lower than that of the optimizer state of global sharding.

Therefore, the order of communication overhead is: no sharding < intra-group sharding < global sharding. There are two main ideas for the trade-off between memory saving and communication overhead as follows:

1. Model sharding saves memory and allows for larger batch sizes, thereby increasing throughput of per GPU. As summarized earlier, saving memory comes at the cost of increased communication. Therefore, we need to balance the impact of these two factors on training speed.
2. Saving memory can free up memory space for other components, which is beneficial to machine learning systems.

In industrial practice, we observe that overall throughput, as a function of memory savings or communication cost, follows non-monotonic, non-convex, and irregular patterns. When balancing these factors, it is not enough to adjust the strategy using a single rule. Since ZeRO, MiSC and ZeRO++ offer limited solutions, it is important to complement them according to the above principles.

3.3 HO-Ring for All-gather and Reduce-scatter

Since the model state is sharded in a GPU cluster, it is necessary to aggregate or scatter these shards for global synchronization, such as the global all-gather for model parameters in ZeRO2 and the global reduce-scatter for gradients in ZeRO3. In the traditional ring of all-gather/reduce-scatter, each GPU sequentially transfers its shard of data to the next GPU. The transmission efficiency of cross-node communication may be a bottleneck affecting model training.

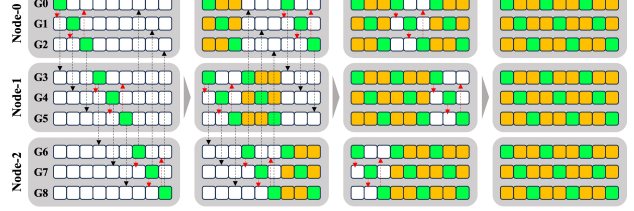


Figure 1. Communication topology of HO-Ring. The N ($N = 9$) GPUs (G_0-G_8) are divided equally into g ($g = 3$) groups. Red and black arrows represent intra- and inter-group communication respectively. Orange and green blocks represent data obtained through intra- and inter-group communication, respectively.

The hierarchical ring (H-Ring) of all-gather/reduce-scatter groups GPUs based on their respective nodes. The global all-gather/reduce-scatter is divided into two steps: intra- and inter-group all-gather/reduce-scatter, to improve inter-group bandwidth utilization and avoid partial GPU waiting. However, during inter-group communication, the intra-group bandwidth is idle, resulting in a waste of resources. Therefore, we proposed a hierarchical overlapping ring (HO-Ring) communication topology for all-gather/reduce-scatter.

Figure 1 shows the communication topology of HO-Ring. Like H-Ring, the GPUs in HO-Ring are also grouped based on their respective nodes. Each GPU transmits its own shards simultaneously through the intra- and inter-group communication rings. Different from the H-Ring, HO-Ring can simultaneously utilize communication resources within and between groups to improve transmission efficiency. In our public cloud experimental environment with 2 machines and 16 workers, the bandwidth of cross-machine communication of a single GPU is only 10~18GB/s, while the aggregate bandwidth of simultaneous cross-machine communication of 8 GPUs is nearly 56GB/s. Therefore, HO-Ring can improve the utilization of bandwidth between groups.

3.4 Gradient Accumulation

Many studies (Li et al., 2021; You et al., 2020) have shown that large batches can effectively improve training efficiency. However, due to limited device memory, the model cannot be fed with very large training batches. The straightforward solution is to divide the large batch into multiple micro-batches, accumulate the gradients generated by each micro-batch, and update parameters only after all micro-batches have been computed. A large amount of communication generated by the global gradient synchronization of each micro-batch will reduce the efficiency of model training. The gradient synchronization range can be narrowed through intra-group gradient backup, thereby reducing the communication volume and number of communications during the training process.

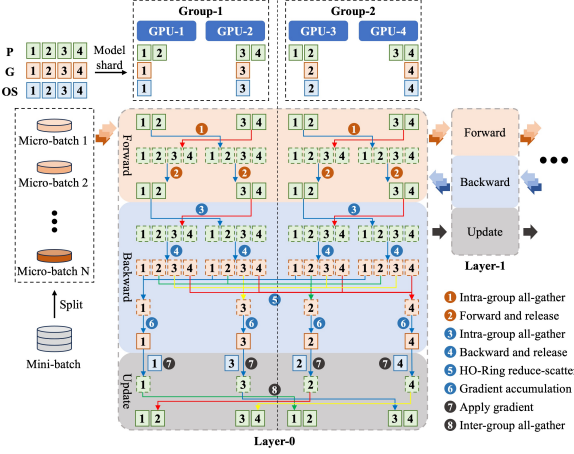


Figure 2. Schematic of PaRO-IGG in a grouped cluster with 4 GPUs. The parameters (P) of the model are sharded within the group, while gradients (G) and optimizer states (OS) are sharded globally. Labeled rectangular blocks represent shards of model parameters, gradients, and optimizer states. The solid and dashed rectangular blocks represent fixed and temporary shards respectively. Circular nodes represent operations in different stages (Forward, Backward, and Update). After feeding a micro-batch, the model will sequentially execute the Forward stage of each layer, followed by the reverse execution of the Backward stage of each layer. The Update stage will only be executed after completing the Backward stage of the last micro-batch.

Specifically, we perform intra-group sharding and inter-group replication of gradients. Each group maintains a complete copy of the gradient. The gradients of each micro-batch are synchronized through the reduce-scatter within the group. After accumulating the gradients from all micro-batches, global gradient synchronization can be achieved by performing an inter-group reduce-scatter operation only once. Compared with the global reduce-scatter, the single-GPU communication volume reduced by the grouped two-step reduce-scatter is as follows:

$$\begin{aligned} \Delta_C = & s * \frac{\Psi}{N} * (N - 1) - \\ & \left(s * \frac{\Psi}{M} * (M - 1) + \frac{\Psi}{N} * (g - 1) \right) \quad (1) \\ = & \frac{\Psi * (s - 1) * (g - 1)}{N} \end{aligned}$$

where, the first item is the communication volume of global reduce-scatter, and the second item is the total communication of intra-group reduce-scatter and inter-group reduce-scatter. It can be observed that as the number of groups g and the accumulation steps s increase, the reduction in communication volume on a single GPU becomes more significant. In the absence of cluster grouping (i.e. $g = 1$) or gradient accumulation (i.e. $s = 1$), there is no reduction in single-GPU communication volume. Therefore, the com-

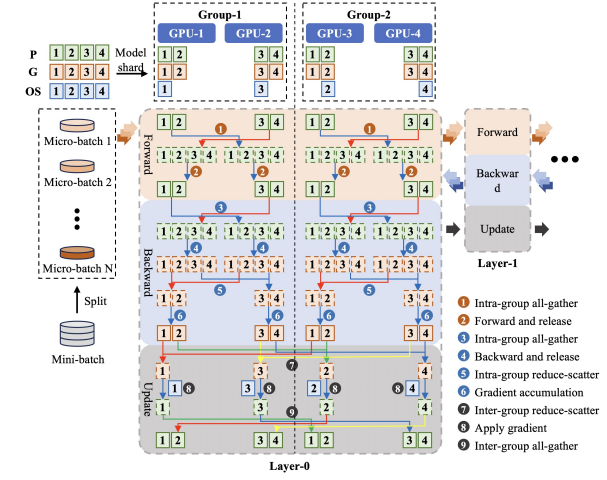


Figure 3. Schematic of PaRO-IIG in a grouped cluster with 4 GPUs.

bination of gradient accumulation and cluster grouping is of practical significance to reduce communication.

3.5 Partial Redundancy Optimizers

Based on ZeRO2 and ZeRO3, we have proposed three optimization schemes, namely PaRO-IGG, PaRO-IIG, and PaRO-NIG, by introducing a small amount of memory redundancy to reduce inter-group communication.

Figure 2 illustrates the model state of PaRO-IGG. To simplify the diagram, we only use 4 GPU devices and divide them into two groups. To reduce inter-group communication frequency and volume, in PaRO-IGG, model parameters are intra-group sharded, while gradients and optimizer states are globally sharded. Therefore, a complete copy of the model parameters is stored within each group. During the training process, a mini-batch is divided into multiple micro-batches to reduce the memory usage for storing activation outputs. In the Forward stage, each GPU obtains a complete backup of model parameters through the intra-group all-gather operation. These model parameters are used to perform the forward computation of the current layer on the input micro-batch, and are later released to reduce GPU memory usage. After completing the Forward stage of the current layer, the system proceeds to the Forward stage of the next layer until the final layer of the network. In the Backward phase, the model parameters are collected again through the intra-group all-gather and released after the backward calculation of this layer. After the backward computation, each GPU obtains a complete copy of the gradients and releases the redundant model parameters. Each GPU aggregates gradients from other GPUs through HO-Ring reduce-scatter operations for global gradient synchronization. In addition, each GPU maintains a gradient shard that

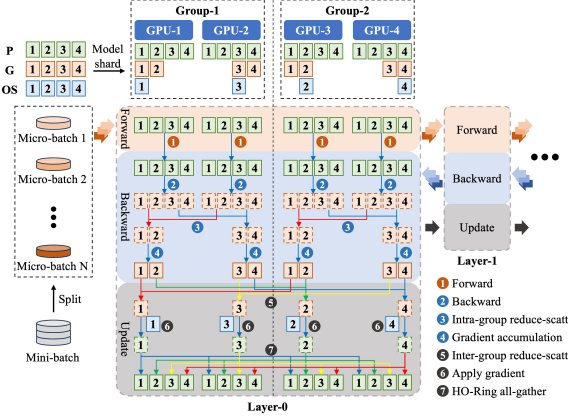


Figure 4. Schematic of PaRO-NIG in a grouped cluster with 4 GPUs.

accumulates gradients generated by each micro-batch. Similarly, after completing the Backward phase of the current layer, the system will execute the Backward phase of the previous layer until the first layer of the network. Once the gradients of the last micro-batch are accumulated, each GPU utilizes the gradient shard to update the optimizer state maintained by itself and generate low-precision model parameters. Finally, model parameter shards are obtained from other groups through an inter-group all-gather operation.

Figure 3 illustrates the model state of PaRO-IIG. Different from PaRO-IGG, in PaRO-IIG, the model parameters and gradients are intra-group sharded, while the optimizer states are globally sharded. Therefore, full model parameters and gradients are preserved within each group. In the Forward and pre-Backward stages, the calculation processes of PaRO-IIG and PaRO-IGG are consistent. After the backward computation, each GPU aggregates gradients from other GPUs through intra-group reduce-scatter operations for local gradient synchronization. These gradients are temporarily stored on each GPU through gradient accumulation. Once the gradients of the last micro-batch are accumulated, each GPU performs an inter-group reduce-scatter operation to achieve global gradient synchronization. The subsequent Update operations are the same as PaRO-IGG.

Figure 4 illustrates the model state of PaRO-NIG. In PaRO-NIG, the parameters of the model are not sharded, the gradients are intra-group sharded, and the optimizer states are global sharded. Different from the above two solutions, each GPU retains complete model parameters in PaRO-NIG. Therefore, in the Forward and Backward stages, each GPU can directly perform the forward and backward calculations without collecting and releasing model parameters. The subsequent four-step calculation process of PaRO-NIG is consistent with that of PaRO-IIG. Finally, each GPU collects updated gradients by HO-Ring all-gather operations.

Table 1. Single-GPU memory usage of parameter P, gradient G and optimizer state OS in different solutions.

Model states	P	G	OS
ZeRO1	2Ψ	2Ψ	$\frac{K\Psi}{N}$
ZeRO2	2Ψ	$\frac{2\Psi}{N}$	$\frac{K\Psi}{N}$
ZeRO3	$\frac{2\Psi}{N}$	$\frac{2\Psi}{N}$	$\frac{K\Psi}{N}$
MiCS	$\frac{2\Psi}{M}$	$\frac{2\Psi}{M}$	$\frac{K\Psi}{M}$
ZeRO++	$\frac{2\Psi}{N} + \frac{2\Psi}{M}$	$\frac{2\Psi}{N}$	$\frac{K\Psi}{N}$
PaRO-IGG	$\frac{2\Psi}{M}$	$\frac{2\Psi}{N}$	$\frac{K\Psi}{N}$
PaRO-IIG	$\frac{2\Psi}{M}$	$\frac{2\Psi}{M}$	$\frac{K\Psi}{N}$
PaRO-NIG	2Ψ	$\frac{2\Psi}{M}$	$\frac{K\Psi}{N}$

3.6 Memory and Communication Analysis

This section analyzes the advantages of the above three solutions in terms of memory usage and communication by comparing other solutions.

Table 1 shows the single-GPU memory usage of parameter P, gradient G and optimizer state OS in different solutions. As can be seen, the single GPU memory usage of ZeRO1, ZeRO2, and ZeRO3 is not affected by the number of groups, as they only perform global sharding operations. MiCS shards the entire model state within the group and introduces inter-group redundancy. As a result, the single-GPU memory of MiCS linearly increases with the number of groups. Based on ZeRO3, ZeRO++ additionally retains the intra-group sharding of model parameters, while PaRO-IGG only retains the intra-group sharding of model parameters. Therefore, the single-GPU memory of PaRO-IGG and ZeRO++ slowly increases with the number of groups. PaRO-IIG shards model parameters and gradients within groups, further increasing memory redundancy. Based on ZeRO2, PaRO-NIG shards gradient groups, and its memory redundancy also increases slowly as the number of groups increases.

Table 2 shows the total communication volume of different solutions in the Forward, Backward and Update stages with a micro-batch input. As can be seen from Table 2, each GPU in ZeRO1 performs gradient accumulation locally, and only performs a global synchronization after gradient accumulation. MiCS performs intra-node communication in the Forward and Backward phases, and only performs a partial gradient all-reduce operation for parameter update. For ZeRO++, due to the secondary intra-node sharding of the collected model parameters in the Forward phase, the parameters can be collected using an intra-node all-gather operation in the Backward phase. Since MiCS, PaRO-IGG and PaRO-IIG shard the model parameters within the group, the all-gather operations in forward and backward calcu-

Table 2. Total communication volume of different solutions in the Forward, Backward and Update stages with a micro-batch input. A-G(P) represents the all-gather operation for the parameter P; R-S(G) and A-G(G) respectively represent the reduce-scatter and all-reduce (**bold**) operations on the gradient G. The \dagger symbol in the upper right corner of the data indicates that the operation is inter-group communication, otherwise it is intra-group communication.

Methods	Forward		Backward		Update	
	A-G(P)	A-G(P)	A-G(P)	R-S(G)	R-S(G)/A-R(G)	A-G(P)
ZeRO1	0	0	0	0	$2 * g * \frac{\Psi}{N} * (N - 1)^\dagger + 2 * (N - g) * \frac{\Psi}{N} * (N - 1)$	$g * \frac{\Psi}{N} * (N - 1)^\dagger + (N - g) * \frac{\Psi}{N} * (N - 1)$
ZeRO2	0	0	$g * s * \frac{\Psi}{N} * (N - 1)^\dagger + (N - g) * s * \frac{\Psi}{N} * (N - 1)$	$(N - g) * s * \frac{\Psi}{N} * (N - 1)$	0	$g * \frac{\Psi}{N} * (N - 1)^\dagger + (N - g) * \frac{\Psi}{N} * (N - 1)$
ZeRO3	$g * s * \frac{\Psi}{N} * (N - 1)^\dagger + (N - g) * s * \frac{\Psi}{N} * (N - 1)$	$g * s * \frac{\Psi}{N} * (N - 1)^\dagger + (N - g) * s * \frac{\Psi}{N} * (N - 1)$	$g * s * \frac{\Psi}{N} * (N - 1)^\dagger + (N - g) * s * \frac{\Psi}{N} * (N - 1)$	$(N - g) * s * \frac{\Psi}{N} * (N - 1)$	0	0
MiCS	$N * s * \frac{\Psi}{M} * (M - 1)$	$N * s * \frac{\Psi}{M} * (M - 1)$	$N * s * \frac{\Psi}{M} * (M - 1)$	$N * s * \frac{\Psi}{M} * (M - 1)$	$2 * g * \frac{\Psi}{M} * (g - 1)^\dagger + 2 * (N - g) * \frac{\Psi}{M} * (g - 1)$	0
ZeRO++	$g * s * \frac{\Psi}{N} * (N - 1)^\dagger + (N - g) * s * \frac{\Psi}{N} * (N - 1)$	$N * s * \frac{\Psi}{M} * (M - 1)$	$g * s * \frac{\Psi}{N} * (N - 1)^\dagger + (N - g) * s * \frac{\Psi}{N} * (N - 1)$	$(N - g) * s * \frac{\Psi}{N} * (N - 1)$	0	0
PaRO-IGG	$N * s * \frac{\Psi}{M} * (M - 1)$	$N * s * \frac{\Psi}{M} * (M - 1)$	$N * s * \frac{\Psi}{N} * (g - 1)^\dagger + N * s * \frac{\Psi}{M} * (M - 1)$	$N * s * \frac{\Psi}{N} * (g - 1)^\dagger + N * s * \frac{\Psi}{M} * (M - 1)$	0	$N * s * \frac{\Psi}{N} * (g - 1)^\dagger$
PaRO-IIG	$N * s * \frac{\Psi}{M} * (M - 1)$	$N * s * \frac{\Psi}{M} * (M - 1)$	$N * s * \frac{\Psi}{M} * (M - 1)$	$N * s * \frac{\Psi}{M} * (M - 1)$	$N * \frac{\Psi}{N} * (g - 1)^\dagger$	$N * \frac{\Psi}{N} * (g - 1)^\dagger$
PaRO-NIG	0	0	0	$N * \frac{\Psi}{M} * (M - 1)$	$N * \frac{\Psi}{N} * (g - 1)^\dagger$	$N * \frac{\Psi}{N} * (g - 1)^\dagger + N * \frac{\Psi}{M} * (M - 1)$

lations are intra-group communications. Compared with ZeRO3, these solutions increase the size of a single transmission ($\frac{\Psi}{M}$ vs. $\frac{\Psi}{N}$) and reduce the number of communications ($s * (M - 1)$ vs. $s * (N - 1)$), which can improve the bandwidth utilization within the group. Compared with ZeRO2, PaRO-NIG splits the global reduce-scatter of the gradient into two steps: intra- and inter-group reduce-scatter through intra-group sharding.

Figure 5 shows the total intra- and inter-group communication volume of different solutions under the condition of $\Psi = 7B$, $N = 64$, $s = 8$, $g = 8$, as well as the memory occupation of a single GPU. As ZeRO1, ZeRO2, and ZeRO3 progressively shard the model state, there is a near-linear reduction in single-GPU memory, while the communication volume both intra- and inter-group increases exponentially. Compared with ZeRO3, the single-GPU memory of ZeRO++, PaRO-IGG and PaRO-IIG increases slightly, while that of MiCS increases significantly; the intra-group communication volume of ZeRO++, PaRO-IGG, and PaRO-IIG is the same as ZeRO3, only slightly increased in MiCS; the inter-group communication volume of MiCS, ZeRO++, PaRO-IGG, and PaRO-IIG is smaller than ZeRO3, with MiCS and PaRO-IIG being the lowest. Compared with ZeRO2, the intra-group communication volume and single-GPU memory of PaRO-NIG increase slightly, while the inter-group communication volume decreases significantly. In addition, the hierarchical communication topology in PaRO utilizes higher inter-group aggregate bandwidth to further improve communication efficiency. In summary, PaRO-IGG, PaRO-IIG, and PaRO-NIG offer a better bal-

ance between memory and communication volume to train large models more efficiently.

4 EXPERIMENTS AND ANALYSIS

In this section, we evaluate the transmission efficiency of the HO-Ring communication topology through data transmission between two nodes. Afterwards, We perform end-to-end training to evaluate the throughput, scalability, and convergence of the proposed PaRO.

4.1 Experiment Environments

Our experimental cluster consists of up to 16 DGX nodes, with each node containing 8 Ampere A100 SXM3 80GB GPUs. The GPUs within each node are interconnected via NVLink/NVSwitch with a bidirectional bandwidth of up to 600GB/s. These nodes are connected through 8 InfiniBand adapters that support NVIDIA SHARP, providing inter-node bandwidth of over 100GB/s. The software environment includes CUDA-11.7, DeepSpeed-v0.10.0, PyTorch-v1.9.2, and nccl-v2.14.3.

4.2 HO-Ring communication performance

In the section, we performed experiments using 2 DGX nodes, with a total communication volume set to 100GB. We measured the communication time of the all-gather operation with the traditional Ring (baseline) and the HO-Ring. The communication times of traditional Ring and HO-Ring are 459ms and 309ms respectively. Compared with the base-

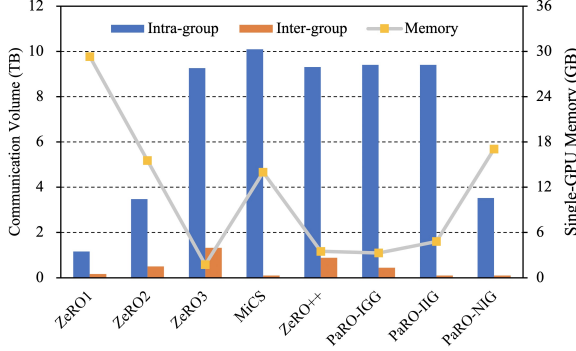


Figure 5. Under the conditions of $\Psi = 7B$, $N = 64$, $s = 8$, $g = 8$, the total communication volume (intra- and inter-group), and single GPU memory of model states.

line Ring method, the communication time of HO-Ring is reduced by 32.6%. Therefore, HO-Ring can significantly improve communication efficiency by improving the communication topology.

4.3 Throughput performance

We used ZeRO2 and ZeRO3 in DeepSpeed as baselines to implement PaROs with different sharding strategies. To evaluate the performance of PaROs, we compared them with current state-of-the-art solutions, including: ZeRO2, ZeRO3, MiCS, ZeRO++, FSDP-hs and FSDP-hsZ2. ZeRO1 was not considered due to its inability to run the smallest scale model in our experiments. We used two LLMs with different parameter sizes: LLaMA-7B and LLaMA-65B (Touvron et al., 2023), to evaluate the throughput and acceleration performance at varying GPU counts. For the LLaMA-65B model, we activate checkpointing to ensure successful training. The C4 corpus in RedPajama is used as the training data set. During training, we set the sequence length to 512, the batch size to 40 (divided into 4 micro-batches), the number of gradient accumulation steps to 10, and mixed precision. All throughput data reported is the average of 100 iterations.

Figure 6 shows the throughput and peak memory of LLaMA-7B and LLaMA-65B models in different solutions. In Figure 6(a), PaRO-IGG outperforms only ZeRO3 and ZeRO++ in terms of throughput; PaRO-IIG achieves higher throughput than MiCS, FSDP-hs, and FSDP-hsZ2; PaRO-NIG shows significantly better throughput than the ZeRO2 baseline. Compared with the baseline ZeRO3, the throughput of PaRO-IGG and PaRO-IIG is improved by 1.3x and 1.9x (with 32 GPUs), 1.4x and 2.6x (with 128 GPUs), respectively. Compared with the baseline ZeRO2, the throughput of PaRO-NIG is improved by 1.7x (with 32 GPUs) and 2.2x (with 128 GPUs), respectively. For the small-scale LLaMA-7B model, both PaRO-IIG and PaRO-NIG approaches show

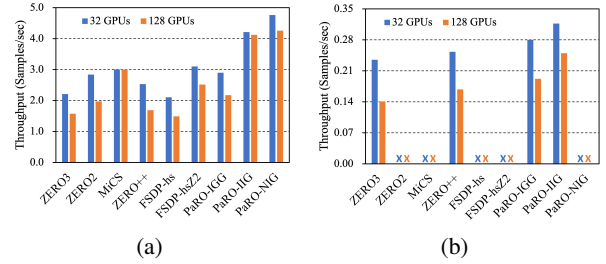


Figure 6. Throughput of LLaMA-7B (a) and LLaMA-65B (b) models in different solutions. The cross indicates OOM.

higher throughput in clusters with 32 and 128 GPUs.

Figure 6(b) presents the single GPU throughput of the LLaMA-65B model with different approaches. Due to the need for finer-grained sharding in the LLaMA-65B model, only ZeRO3, ZeRO++, PaRO-IGG, and PaRO-IIG were able to complete the training, while other approaches encountered out-of-memory (OOM) issues. Compared with the baseline ZeRO3, the throughput of PaRO-IGG and PaRO-IIG is improved by 1.2x and 1.3x (with 32 GPUs), 1.4x and 1.8x (with 128 GPUs), respectively. For the large-scale LLaMA-65B model, training efficiency is higher with the PaRO-IGG and PaRO-IIG compared to the ZeRO3.

4.4 Near-linear Scalability

To analyze the relationship between throughput and GPU resources, we collected data on the single-GPU throughput of the PaROs and two baselines at different numbers of GPU, as shown in Figure 7. The experiments were conducted using the LLaMA-7B model. Overall, under the same GPU resource conditions, the single-GPU throughput of PaRO is higher than the baseline ZeRO2 and ZeRO3. The single-GPU throughput of different approaches gradually decreases as the number of GPUs increases. The throughput of PaRO-IIG decreases the least, and the throughput of ZeRO2 decreases the most. Due to network instability, the throughput ratios of ZeRO3 and PaRO-IGG fluctuate greatly. Therefore, as the cluster size increases, PaRO-IIG can maintain near-linear scalability.

4.5 Model Convergence

In this section, we show that PaRO achieves consistent convergence as ZeRO, which validates the correctness of our system. We used LLaMA-7B model and C4 corpus in RedPajama to evaluate the convergence of PaRO. During training, we set the sequence length to 128, the batch size to 1024 (divided into 8 micro-batches) and the number of gradient accumulation steps to 10. The loss validation process does not aim to produce exactly the same loss as DeepSpeed but to ensure the convergence behaviours are the same. As

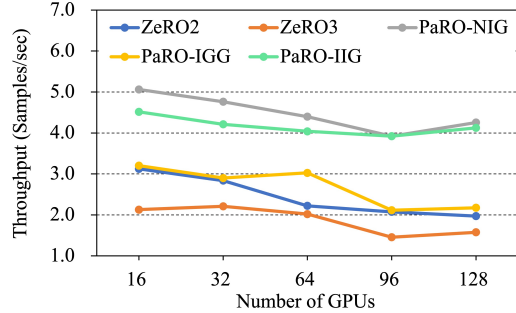


Figure 7. Throughput with different number of GPUs.

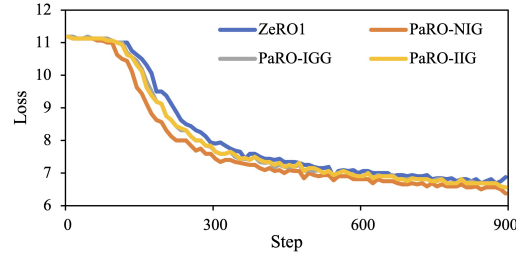


Figure 8. Training convergence for LLaMA-7B.

shown in Figure 8, PaRO provides the same convergence as ZeRO.

5 CONCLUSION

In this paper, we present PaRO, a system that provides more refined options for the trade-off between memory occupation and communication overhead in different training scenarios. PaRO reduces the amount and frequency of inter-group communication by grouping GPU clusters and introducing minor intra-group memory redundancy, thereby improving the training efficiency of the model. Additionally, we propose a HO-Ring communication topology to enhance communication efficiency between nodes or across switches in large model training. We evaluate PaRO on various training workloads on large-scale clusters. PaRO outperforms ZeRO by up to 2.6 \times and demonstrates near-linear scalability in various training setups.

REFERENCES

Agarwal, R. C., Balle, S. M., Gustavson, F. G., Joshi, M., and Palkar, P. A three-dimensional approach to parallel matrix multiplication. *IBM Journal of Research and Development*, 39(5):575–582, 1995. doi: 10.1147/rd.395.0575.

Bian, Z., Xu, Q., Wang, B., and You, Y. Maximizing parallelism in distributed training for huge neural networks, 2021.

Brown, T., Mann, B., Ryder, N., Subbiah, M., Kaplan, J. D., Dhariwal, P., Neelakantan, A., Shyam, P., Sastry, G., Askell, A., Agarwal, S., Herbert-Voss, A., Krueger, G., Henighan, T., Child, R., Ramesh, A., Ziegler, D., Wu, J., Winter, C., Hesse, C., Chen, M., Sigler, E., Litwin, M., Gray, S., Chess, B., Clark, J., Berner, C., McCandlish, S., Radford, A., Sutskever, I., and Amodei, D. Language models are few-shot learners. In Larochelle, H., Ranzato, M., Hadsell, R., Balcan, M., and Lin, H. (eds.), *Advances in Neural Information Processing Systems*, volume 33, pp. 1877–1901. Curran Associates, Inc., 2020.

Devlin, J., Chang, M.-W., Lee, K., and Toutanova, K. Bert: Pre-training of deep bidirectional transformers for language understanding, 2019.

Fan, S., Rong, Y., Meng, C., Cao, Z., Wang, S., Zheng, Z., Wu, C., Long, G., Yang, J., Xia, L., Diao, L., Liu, X., and Lin, W. Dapple: A pipelined data parallel approach for training large models. In *Proceedings of the 26th ACM SIGPLAN Symposium on Principles and Practice of Parallel Programming, PPoPP ’21*, pp. 431–445, New York, NY, USA, 2021. Association for Computing Machinery. ISBN 9781450382946. doi: 10.1145/3437801.3441593.

Huang, Y., Cheng, Y., Bapna, A., Firat, O., Chen, M. X., Chen, D., Lee, H., Ngiam, J., Le, Q. V., Wu, Y., and Chen, Z. Gpipe: Efficient training of giant neural networks using pipeline parallelism, 2019.

Jia, X., Song, S., He, W., Wang, Y., Rong, H., Zhou, F., Xie, L., Guo, Z., Yang, Y., Yu, L., et al. Highly scalable deep learning training system with mixed-precision: Training imagenet in four minutes. *arXiv preprint*, 2018.

Kingma, D. P. and Ba, J. Adam: A method for stochastic optimization, 2017.

Korthikanti, V. A., Casper, J., Lym, S., McAfee, L., Anderesch, M., Shoeybi, M., and Catanzaro, B. Reducing activation recomputation in large transformer models. *Proceedings of Machine Learning and Systems*, 5, 2023.

Li, C., Awan, A. A., Tang, H., Rajbhandari, S., and He, Y. 1-bit lamb: Communication efficient large-scale large-batch training with lamb’s convergence speed, 2021.

Li, S., Liu, H., Bian, Z., Fang, J., Huang, H., Liu, Y., Wang, B., and You, Y. Colossal-ai: A unified deep learning system for large-scale parallel training. In *Proceedings of the 52nd International Conference on Parallel Processing, ICPP ’23*, pp. 766–775, New York, NY, USA, 2023. Association for Computing Machinery. ISBN 9798400708435. doi: 10.1145/3605573.3605613.

Mikami, H., Suganuma, H., U-chupala, P., Tanaka, Y., and Kageyama, Y. Massively distributed sgd:

Imagenet/resnet-50 training in a flash. *arXiv preprint*, 2018.

Narayanan, D., Shoeybi, M., Casper, J., LeGresley, P., Patwary, M., Korthikanti, V., Vainbrand, D., Kashinkunti, P., Bernauer, J., Catanzaro, B., Phanishayee, A., and Zaharia, M. Efficient large-scale language model training on gpu clusters using megatron-lm. In *Proceedings of the International Conference for High Performance Computing, Networking, Storage and Analysis*, SC '21, New York, NY, USA, 2021. Association for Computing Machinery. ISBN 9781450384421. doi: 10.1145/3458817.3476209.

Proficz, J. Improving all-reduce collective operations for imbalanced process arrival patterns. *The Journal of Supercomputing*, 74(7):3071–3092, July 2018. ISSN 1573-0484. doi: 10.1007/s11227-018-2356-z.

Rajbhandari, S., Rasley, J., Ruwase, O., and He, Y. Zero: Memory optimizations toward training trillion parameter models. In *Proceedings of the International Conference for High Performance Computing, Networking, Storage and Analysis*, SC '20. IEEE Press, 2020. ISBN 9781728199986.

Rajbhandari, S., Ruwase, O., Rasley, J., Smith, S., and He, Y. Zero-infinity: Breaking the gpu memory wall for extreme scale deep learning. In *Proceedings of the International Conference for High Performance Computing, Networking, Storage and Analysis*, SC '21, New York, NY, USA, 2021. Association for Computing Machinery. ISBN 9781450384421. doi: 10.1145/3458817.3476205.

Ren, J., Rajbhandari, S., Aminabadi, R. Y., Ruwase, O., Yang, S., Zhang, M., Li, D., and He, Y. Zero-offload: Democratizing billion-scale model training, 2021.

Sergeev, A. and Balso, M. D. Horovod: fast and easy distributed deep learning in tensorflow, 2018.

Shoeybi, M., Patwary, M., Puri, R., LeGresley, P., Casper, J., and Catanzaro, B. Megatron-lm: Training multi-billion parameter language models using model parallelism, 2020.

Solomonik, E. and Demmel, J. Communication-optimal parallel 2.5d matrix multiplication and lu factorization algorithms. In Jeannot, E., Namyst, R., and Roman, J. (eds.), *Euro-Par 2011 Parallel Processing*, pp. 90–109, Berlin, Heidelberg, 2011. Springer Berlin Heidelberg. ISBN 978-3-642-23397-5.

Touvron, H., Lavril, T., Izacard, G., Martinet, X., Lachaux, M.-A., Lacroix, T., Rozière, B., Goyal, N., Hambro, E., Azhar, F., et al. Llama: Open and efficient foundation language models. *arXiv preprint*, 2023.

Wang, B., Xu, Q., Bian, Z., and You, Y. 2.5-dimensional distributed model training. *arXiv e-prints*, pp. arXiv-2105, 2021.

Wang, G., Venkataraman, S., Phanishayee, A., Devanur, N., Thelin, J., and Stoica, I. Blink: Fast and generic collectives for distributed ml. *Proceedings of Machine Learning and Systems*, 2:172–186, 2020.

Wang, G., Qin, H., Jacobs, S. A., Holmes, C., Rajbhandari, S., Ruwase, O., Yan, F., Yang, L., and He, Y. Zero++: Extremely efficient collective communication for giant model training, 2023.

Xu, Q. and You, Y. An efficient 2d method for training super-large deep learning models. In *2023 IEEE International Parallel and Distributed Processing Symposium (IPDPS)*, pp. 222–232, 2023. doi: 10.1109/IPDPS54959.2023.00031.

You, Y., Li, J., Reddi, S., Hseu, J., Kumar, S., Bhojanapalli, S., Song, X., Demmel, J., Keutzer, K., and Hsieh, C.-J. Large batch optimization for deep learning: Training bert in 76 minutes, 2020.

Zhang, Z., Zheng, S., Wang, Y., Chiu, J., Karypis, G., Chilimbi, T., Li, M., and Jin, X. Mics: Near-linear scaling for training gigantic model on public cloud. *Proc. VLDB Endow.*, 16(1):37–50, sep 2022. ISSN 2150-8097. doi: 10.14778/3561261.3561265.

Zhao, Y., Gu, A., Varma, R., Luo, L., Huang, C.-C., Xu, M., Wright, L., Shojanazeri, H., Ott, M., Shleifer, S., Desmaison, A., Balioglu, C., Damania, P., Nguyen, B., Chauhan, G., Hao, Y., Mathews, A., and Li, S. Pytorch fsdp: Experiences on scaling fully sharded data parallel. *Proc. VLDB Endow.*, 16(12):3848–3860, sep 2023. ISSN 2150-8097. doi: 10.14778/3611540.3611569.